Colloids and Surfaces B: Biointerfaces 218 (2022) 112749

Contents lists available at ScienceDirect

Colloids and Surfaces B: Biointerfaces

journal homepage: www.elsevier.com/locate/colsurfb

Precipitation of calcium carbonate in the presence of rhamnolipids in alginate hydrogels as a model of biomineralization

Natalia Czaplicka [a,*], Donata Konopacka-Łyskawa [a], Agata Nowotnik [a], Aleksandra Mielewczyk-Gryń [b], Marcin Łapiński [b], Rafał Bray [c]

[a] Department of Process Engineering and Chemical Technology, Faculty of Chemistry, Gdańsk University of Technology, Narutowicza 11/12, 80-233 Gdańsk, Poland
[b] Institute of Nanotechnology and Materials Engineering and Advanced Materials Center, Faculty of Applied Physics and Mathematics, Gdańsk University of Technology, Narutowicza 11/12, 80-233 Gdańsk, Poland
[c] Department of Water and Wastewater Technology, Faculty of Civil and Environmental Engineering, Gdańsk University of Technology, Narutowicza 11/12, 80-233 Gdańsk, Poland

ARTICLE INFO

Keywords:
Calcium carbonate
Precipitation
Alginate hydrogel
Biomineralization
Rhamnolipids

ABSTRACT

This paper reports the effects of rhamnolipids presence in the alginate hydrogel and CO_3^{2-} solution, on the precipitation of $CaCO_3$ in the Ca^{2+} loaded alginate hydrogel. Characteristics of the formed particles are discussed. Model conditions containing alginate hydrogel and rhamnolipids were used in order to mimic the natural environment of biomineralization in biofilms. It has been shown that rhamnolipids affect the characteristics of precipitated calcium carbonate effect of using these biosurfactants depends on their concentration as well as whether they are directly present in the hydrogel matrix or the carbonate solution surrounding the hydrogel. The greatest effect compared to the control samples was found for the rhamnolipids in the form of micelles directly present in the hydrogel with the $CaCl_2$ cross-linked solution at concentration of 0.05 M. These conditions result in the highest increase in vaterite content, specific surface area, and pore volume. The mechanism of $CaCO_3$ precipitation in alginate hydrogel containing rhamnolipids has been proposed.

1. Introduction

Biomineralization is a multistage process carried out by living organisms. It includes the selective capture of individual components from the local environment and their transformation into crystal structures under specified biological control. Therefore, this process is a consequence of cellular activity that allows for physicochemical changes necessary for crystal growth and formation of biominerals [1–3]. Biominerals are minerals with the co-existing organic phase. The occurrence of the organic matrix is caused by its passive and active participation in the formation of biominerals, and then its gradual incorporation into the structure of the growing skeleton. Passive participation consists in creating a space in which the solution is supersaturated relative to the ions involved in the biomineralization, while the active participation is caused by structural and chemical interactions that promote the formation of biominerals with specific properties [4]. In order to produce minerals, living organisms create a microenvironment in which crystal growth with species-specific morphology is possible. The driving force of the crystallization process is the supersaturation of the solution. Thus, the first stage of biominerals crystallization is the dissolution of individual ions in the solvent, or their passage to the solvent, which may be the body fluid of the living organism or, in the case of bacteria, the external environment. A supersaturated solution is then created, followed by nucleation and crystal growth. The first two stages depend mainly on the solubility product of the salt that forms the crystal structure. Nucleation and crystal growth up to the given polymorphic form are more complicated in the biological systems. The concentrations of individual ions, as well as the content of organic and inorganic components in such microenvironment, are values that change rapidly over time, making their measurements very complicated. For this reason, in the case of biomineralization, references are made to the basic mechanisms of crystal formation in simple non-biological systems that are well known and characterized. Therefore, an important source of knowledge about the mechanism of biomineralization are the in vitro studies [2].

Calcium carbonate is one of the most common compound used by living organisms to produce mineral structures. There are three anhydrous polymorphic forms of calcium carbonate i.e. calcite, aragonite,

* Corresponding author.
E-mail address: natalia.czaplicka@pg.edu.pl (N. Czaplicka).

https://doi.org/10.1016/j.colsurfb.2022.112749
Received 19 April 2022; Received in revised form 27 July 2022; Accepted 1 August 2022
Available online 2 August 2022

and vaterite. The most thermodynamically stable, and hence the most common form, is calcite [5]. Its crystals most often take rhombohedral and scalenohedral forms, while the aragonite crystals usually occur in orthorhombic form. Both calcite and aragonite are usually monocrystalline particles. However, the least thermodynamically stable vaterite crystallizes in the form of polycrystalline spherical particles, which an aqueous solutions slowly dissolve and recrystallize to the other two more stable polymorphs [6,7]. Below 40 °C, the conversion occurs to the most thermodynamically stable calcite, while at higher temperatures vaterite is transformed into aragonite [8]. As a result of the lower thermodynamic stability, aragonite and vaterite are less common as natural minerals compared to calcite. However, in biological systems, these polymorphs can nucleate and grow stably. The mechanism of interaction between calcium carbonate polymorphs and complex organic matrices is of interest to scientists from various fields. This is because organisms use macromolecular matrices such as polysaccharides, proteins, and acidic biomacromolecules, or amphiphilic complexes, to modulate the formation of inorganic minerals [9,10]. The addition of these molecules to the reaction system results in the formation of particles with different morphologies, sizes, and polymorphic compositions [11].

Interesting compounds that may have a potential influence on the biominerals production are biosurfactants because they contain functional groups that can bind to metal ions and the surfaces of mineral particles in aqueous solutions [12,13]. These biomolecules play a significant role in the mobility and formation of biofilms by bacterial cells and they also increase the solubility and bioavailability of hydrophobic compounds. The most numerous group of organisms capable of synthesizing biosurfactants are microorganisms, mainly bacteria and yeasts [14]. In the literature, research on certain biosurfactants, such as surfactin lipopeptide [15–17] and phospholipids [18–21], for calcium carbonate precipitation can be found. Despite the intensive research on the $CaCO_3$ precipitation in the context of biomineralization, mono- and di-rhamnolipids have not been used as additives to the precipitation system until now. These biosurfactants are classified as glycolipids and consist of a mono- or disaccharide molecule connected by a glycosidic bond with a fatty acid. Rhamnolipids contain one or two rhamnose rings connected to β-hydroxydecanoic acid and they are synthesized mainly by *Pseudomonas aeruginosa*.

Biomineralization carried out by microorganisms is an ubiquitous process that occurs in almost all natural environments [22]. According to numerous studies, at least 200 types of bacteria are involved in the calcium carbonate biomineralization, including *Pseudomonas* [23]. Microorganisms produce a variety of metabolites that change the chemical composition of the biofilm and the surrounding environment, leading to favorable conditions for the precipitation of carbonate minerals. It has also been shown that biofilms of heterogeneous structure with aggregation of attached microorganisms to the surface of cells play a significant role in the biomineralization process [24]. Furthermore, it was found that biomineralization usually occurs in biofilms [24]. Bacteria produce biofilm substances, such as alginate [25], having negatively charged functional groups. These groups act as the $CaCO_3$ nucleation centers by attracting calcium ions, which result in their accumulation. Furthermore, there is a literature evidence on the relationship between rhamnolipids and bacterial biofilm. According to Davey et al. [26], rhamnolipids are responsible for maintaining the functionality of transport channels and affect the structure of the biofilm [27]. In addition, these biosurfactants induce the breakdown of bacterial biofilms and also affect their structure during the early stages of formation and subsequent maturation [28]. Therefore, even though it has not been shown that rhamnolipids occur directly in the structure of biominerals, their presence in the reaction environment may have an impact on the calcium carbonate biomineralization process and the characteristics of the crystals obtained.

Studies available in the literature do not concern the impact of rhamnolipids on calcium carbonate precipitation. This work aims to determine the effect of rhamnolipids present directly in alginate hydrogel and in the CO_3^{2-} solution on the $CaCO_3$ precipitation taking place in the Ca^{2+} loaded alginate hydrogel, and on the characteristics of formed particles. The environment contains alginate hydrogel and rhamnolipids was used as a model matrix because alginate and rhamnolipids are produced by *Pseudomonas* in biofilms [25]. The proposed reaction conditions mimic the natural environment of biomineralization in biofilms. The results of these studies allow to determine the conditions conducive to the formation of the crystalline phase in conditions similar to those occurring in the biofilm.

2. Materials and methods

2.1. Materials

Sodium alginate (Sigma-Aldrich, a viscosity of 1% wt. solution in water at 25 °C: 5–40 mPa·s, M/G ratio: 1.56), anhydrous calcium chloride (≥99.9%, POCH, Poland), anhydrous sodium carbonate (≥99.9%, POCH, Poland), commercial rhamnolipid biosurfactant (R90, 90% purity, AGAE Technologies LLC, Corvallis, OR, USA), methanol (≥99.9%, POCH, Poland), di-sodium wersenate, standard solution 0.1 mol/L (≥99.9%, Chempur, Poland), buffer solution pH 10 ± 0.05 (≥99.9%, Chempur, Poland), eriochrome black T (≥99.9%, Chempur, Poland). Reagents were used without further purification. All solutions were prepared using distilled water.

2.2. CMC determination

The critical micelle concentration CMC values of rhamnolipids in 0.15 mol/L Na_2CO_3 aqueous solution and in 2%wt. alginate aqueous solution at room temperature (22 °C) were determined by measuring the surface tension using a K11 tensiometer (KRÜSS, Hamburg, Germany). The rhamnolipids concentration range was from 10^{-3} to 10^{6} mg/m^3 and each measurement was made in triplicate, and the average was calculated. A surface tension curve versus the decimal logarithm of the biosurfactant concentration was made, from which the CMC value was determined by extrapolating to the cross point of linear relationships from the area of low- and high-concentration [29,30].

2.3. Hydrogels preparation

Alginate hydrogels were prepared by ionic cross-linking of sodium alginate using aqueous solutions of $CaCl_2$ with various concentrations of 0.05, 015, and 0.25 mol/L. Solutions of sodium alginate in distilled water (10 g per 0.5 L of water) were prepared with and without the addition of rhamnolipids. The biosurfactant concentrations were above CMC, equal to CMC, and below CMC. The alginate solutions were poured into the dialysis membrane (VISKING® dialysis tubing made from regenerated cellulose, pore diameter ca. 25 Å, MWCO 12 000–14 000) and placed in the $CaCl_2$ solution for 120 h. Samples (0.002 L) of the $CaCl_2$ solution were collected after 0, 12, 24, 36, 48, 84 and 120 h of crosslinking to determine the concentration of Ca^{2+} ions by complexometric titration with EDTA. The hydrogels that were used as a calcium ion sources for the precipitation of $CaCO_3$ were ionically crosslinked as described above for 24 h.

2.4. CaCO3 precipitation

The single diffusion solution phase reactant method, characterized by mild precipitation conditions, mapping the process of biomineralization in living organisms, has been used to precipitate calcium carbonate. Alginate hydrogels crosslinked with calcium ions were pulled from the dialysis membrane and rinsed with distilled water. The hydrogels were then placed in an aqueous 0.15 M Na_2CO_3 solution and left for 3 days to precipitate calcium carbonate. Precipitation was carried out with the use of hydrogels containing rhamnolipids and pure

Na_2CO_3 and with the use of pure hydrogels and Na_2CO_3 solution with the addition of rhamnolipids with a concentration below CMC, equal to CMC and above CMC. The pH of the reaction mixture during the precipitation process was in the range of 10–10.5. After 3 days, the obtained $CaCO_3$ particles were filtered, washed with methanol, and dried at 90 °C for 24 h (Fig. 1).

2.5. Particles characterization

The conventional powder X-ray diffraction technique (XRD) with Cu-Kα radiation was applied using the MiniFlex 600 diffractometer (Rigaku, Tokyo, Japan) to characterize the polymorphic composition of precipitated $CaCO_3$. XRD analysis was carried out at room temperature, 2θ angle range of 20–80°, and at a scan rate of 0.2°. To identify the types of chemical bonds, Fourier transform infrared spectroscopy (FT-IR) was applied using the Nicolet 8700 Spectrometer (Thermo Scientific, Waltham, MA, USA). The attenuated total reflection (ATR) method was used. Spectra were registered from 4500 to 524 cm^{-1} at 2 cm^{-1} resolution using air as the background. A thermogravimetry analysis (TGA) was performed to determine whether there are organic residues in the samples. TGA was carried out on approximately 10–15 mg of powder, using Netzsch TG 209 F3 Tarsus® (Selb, Germany) thermobalance in nitrogen (40 ml/min purge gas, 20 ml/min protective gas) up to 900 °C with a heating rate of 5°/min. Before the experiment, a blank run on an empty crucible was undertaken to take to account the buoyancy and thermal drift of the thermobalance. The specific surface area and pore size of the $CaCO_3$ particles obtained were determined using the Brunauer-Emmett-Teller (BET) method and were evaluated from the adsorption-desorption isotherms of liquid nitrogen (77 K) detected using the Gemini V Surface Area Analyzer (model 2365, Micromeritics, Norcross, GA, USA). Before measuring, the samples were dried and degassed for 2 h at 200 °C. Specific surface areas were calculated using the BET linear equation in the approximate relative pressure (p/p_0) range of 0.05–0.3. The total pore volume was evaluated from the amount of adsorbed nitrogen at $p/p_0 = 0.995$ (the last adsorption point). The size of precipitated particles was determined by a laser diffraction method using the Mastersizer 2000 analyzer (Malvern Panalytical Ltd., Malvern, United Kingdom) equipped with a standard dispersion units Hydro 2000MU with an ultrasonic probe supporting the breaking of agglomerates. The particle diameter measurement range was between 0.02 and 2000 μm. To characterize the morphology of the $CaCO_3$ particles obtained, a FEI Quanta FEG 250 scanning electron microscope (SEM) equipped with an Large Field Detector (LFD) secondary electron detector at low vacuum conductions (FEI, Hillsboro, OR, USA) was applied.

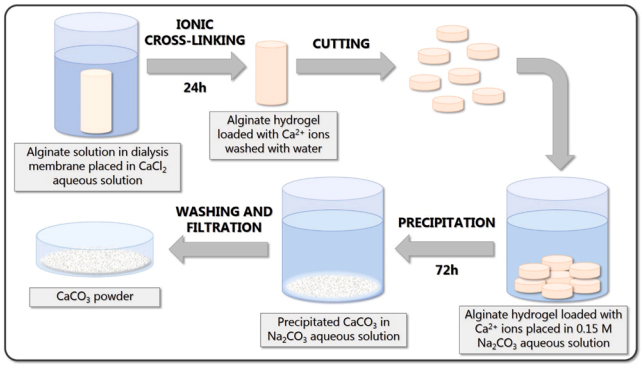

Fig. 1. Scheme of the experimental methodology.

3. Results and discussion

3.1. CMC of rhamnolipids

The dependence of the surface tension on the concentration of rhamnolipids was determined for the solutions with the addition of 0.15 mol/L Na_2CO_3 and 2% wt. alginate, which corresponded to the concentrations of the additives used in this work (see Fig. 2). The most diluted solution of RLs and Na_2CO_3 had surface tension values of 58.9 mN/m, and the RLs and alginate solution of 68.6 mN/m. As the concentration of RLs in the solution increased, the surface tension decreased to a value of 28.7 mN/m in the presence of sodium carbonate and a value of 29.9 mN/m in the presence of alginate. Moreover, in the case of solutions with alginate, the course of the dependence of the surface tension on the rhamnolipid concentration shows an additional lowering of surface tension at rhamnolipid concentrations of about 0.3 mg/L. Similar results were obtained for cationic surfactants in the presence of alginate [31].

The breakpoint in the $\gamma = f(\log C)$ plot is related to the formation of micelles, and the determined critical micellar concentration was 33.11 mg/L for measurements with Na_2CO_3 and 421.7 mg/L with alginate, respectively. Since rhamnolipids are metabolites produced by microorganisms, they are usually a mixture of mono- and di-rhamnolipid homologs [32]. Therefore, the measured results of the critical micellar concentration and the minimum surface tension reported for the rhamnolipid solutions are very diverse. The range of reported CMC values is between 4 and 420 mg/L [33,34], while the surface tension reaches values between 25 and 36 mN/m when the CMC is exceeded [32,34,35]. Although İkizler et al. [36] showed that the ratio of di-RLs to mono-RLs slightly influenced the CMC value. However, the CMC values depend on the pH of the solution and the presence of electrolytes. An increase in pH results in an increase in the concentration at which micelles are formed [35,37]. This is related to the pKa values of rhamnolipids (pKa=5.9 mono-RLs [38] and pKa= 5.6 for di-RLs [35]), therefore at higher pH, the rhamnolipids molecules are negatively charged and the association into micellar aggregates is more difficult [35,38]. However, the addition of electrolyte decreased the CMC value in the slightly alkaline solutions, significantly [38]. In this work, the obtained CMC value for measurements in the presence of Na_2CO_3 is lower than in the case of aqueous solutions without additives, when

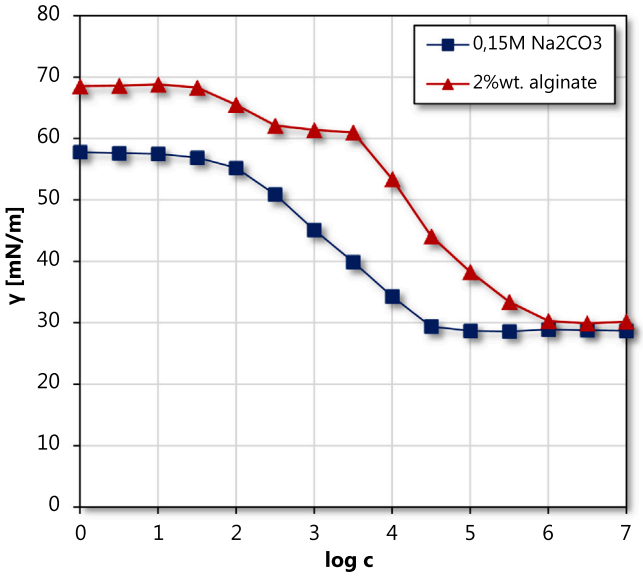

Fig. 2. Surface tension function versus the decimal logarithm of the rhamnolipids concentration at room temperature in 0.15 mol/L Na_2CO_3 and 2% wt. alginate.

CMC was 43.21 mg/L [39]. Although the addition of Na_2CO_3 raises the pH to 11.75, the increase in the ionic strength of the solution has a greater effect on the CMC value. In contrast, the CMC value is much higher when the alginate was an additive. This is probably because the addition of alginate impedes the formation of agglomerates. A similar value was obtained for crude rhamnolipids (CMC = 420 mg/L) [34], then most likely the medium components bound to the RLs molecules, hindering the formation of micelles.

3.2. Changes of Ca^{2+} concentration during ionic cross-linking of hydrogels

The carboxyl and hydroxyl groups present on the surface of the organic matrix provide abundant Ca^{2+} ion binding sites [47]. Thus, the ionic cross-linking of sodium alginate, which in turn leads to the formation of a hydrogel, takes place through the gradual exchange of sodium ions with calcium ions and is readily accomplished by placing an alginate solution in a calcium chloride solution. Then, monovalent Na^+ ions that interact with only one carboxyl group of the alginate changed into divalent Ca^{2+} ions that interact with two carboxyl groups. Based on data from the literature, $CaCl_2$ concentrations of 0.05, 0.15, and 0.25 mol/L were applied in this study. The ion cross-linking of alginate hydrogels was performed with and without the addition of rhamnolipids (RL) using selected concentrations of $CaCl_2$, and the changes in the concentration of Ca^{2+} ions during this process were measured. Fig. 3 presents Ca^{2+} concentration versus time of ion cross-linking curves for all used $CaCl_2$ and rhamnolipid concentrations and the percentage consumption of calcium ions depending on cross-linking time.

The concentration of calcium chloride affects both the physical and mechanical properties of the hydrogels and the rate of cross-linking [48]. Using too low a $CaCl_2$ concentration results in obtaining very soft and incompletely solidified hydrogels. However, too high a concentration of Ca^{2+} ions leads to a very fast cross-linking on the surface of the hydrogel, which hinders the diffusion of divalent ions to deeper

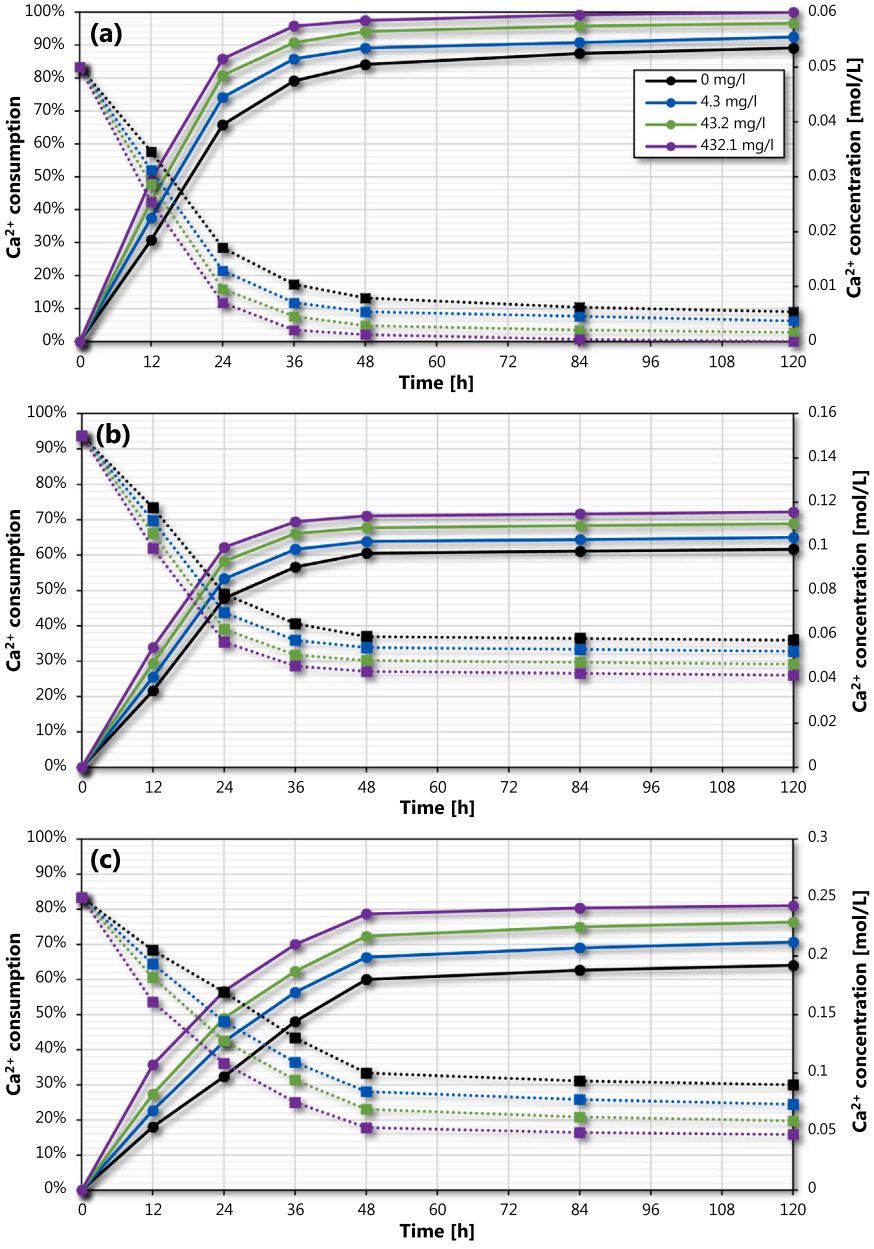

Fig. 3. Ca^{2+} concentration (··■··) and percentage Ca^{2+} consumption (—•—) versus ion cross-linking time curves for different RLs concentrations depending on the $CaCl_2$ concentration: (a) 0.05 M, (b) 0.15 M, and (c) 0.25 M.

layers. As a consequence, selecting too high a $CaCl_2$ concentration leads to the formation of heterogeneous hydrogels, which are very hard on the outside and very soft on the inside. This is confirmed by the results of the percentage consumption of Ca^{2+} ions. The higher the concentration of $CaCl_2$ in the tested range, the lower the consumption of calcium ions during crosslinking for 12 and 24 h. However, after 120 h, higher Ca^{2+} consumption is observed in the case of using 0.25 M $CaCl_2$ compared to 0.15 M. In the graphs presented in Fig. 2 it can be seen that during cross-linking in 0.25 M $CaCl_2$ solution, the decrease in calcium ion concentration occurs slower than in lower concentrations, which is caused by faster hardening of the gel on the surface and hindering the diffusion of ions into the hydrogel. However, the concentration is not too high because further cross-linking up to 120 h results in a continuous decrease in the value of Ca^{2+} concentration, which shows that diffusion occurs throughout this period. According to observations during the experiments, it can also be stated that the concentration of 0.05 M is too low because, despite the almost complete consumption of the calcium ions present in the solution, low-density hydrogels are obtained. Moreover, rhamnolipids present in the hydrogel can bind metal ions [49,50]. These biosurfactants interact with the hydrophobic part of the alginate copolymer chains, and then the hydrophilic groups of adsorbed biosurfactant molecules create additional calcium ion trapping sites. Therefore, for higher concentrations of rhamnolipids, it is possible to introduce more calcium ions that cross-link the alginate molecules.

3.3. $CaCO_3$ particles characterization

3.3.1. Polymorphic composition

The X-ray diffractograms of calcium carbonate obtained with the use of a hydrogel containing rhamnolipids and an aqueous solution of Na_2CO_3 with the addition of biosurfactant are presented in the Supplementary Materials in Figs. S1 and S2, respectively. The characteristic sharp peaks of calcium carbonate in the form of calcite and vaterite are visible in the XRD patterns. This proves the only crystalline phase in the obtained samples. When the samples contain amorphous calcium carbonate, the resulting XRD pattern has a characteristic jagged course [51]. Based on the data obtained and using the method [52] applied in the previous works [53–55], the percentage of vaterite content in the samples was calculated. Fig. 4 presents graphs showing the percentage vaterite content values depending on the concentrations of rhamnolipids and $CaCl_2$.

In the case of the control samples without the addition of rhamnolipids, the following relationship is visible: the higher the $CaCl_2$ concentration, the higher the vaterite content in the precipitated $CaCO_3$. The same trend can be seen for all other series of experiments using different concentrations of rhamnolipids, except for the series of precipitations with a hydrogel containing RLs above the CMC concentration. Then, an increase in $CaCl_2$ concentration results in a decrease in the vaterite content.

On the other hand, in the case of 0.05 M $CaCl_2$, an increase in the RLs concentration both in the hydrogel and the Na_2CO_3 solution, increases in the vaterite content. However, for 0.15 and 0.25 M of $CaCl_2$, the addition of RLs to the hydrogel at a concentration below and in CMC causes a decrease in X_v, while at a concentration higher than CMC, an increase in X_v compared to the control samples. The situation is different when rhamnolipids are present in the Na_2CO_3 solution. Then the reduction of the vaterite content occurs only for concentrations below the CMC. The use of a concentration equal to or higher than the CMC results in the obtaining of $CaCO_3$ that contains more vaterite than the control samples.

3.3.2. Organic residues

Figs. S3 and S4 show the FTIR-ATR spectra of all obtained calcium carbonate particles. In the case of calcium carbonate, there are three characteristic absorption bands. The symmetrical stretching from the oscillation of the C–O bond is responsible for the first one, which is in the range of 1000–1100 cm^{-1}. The second band comes from the out-of-

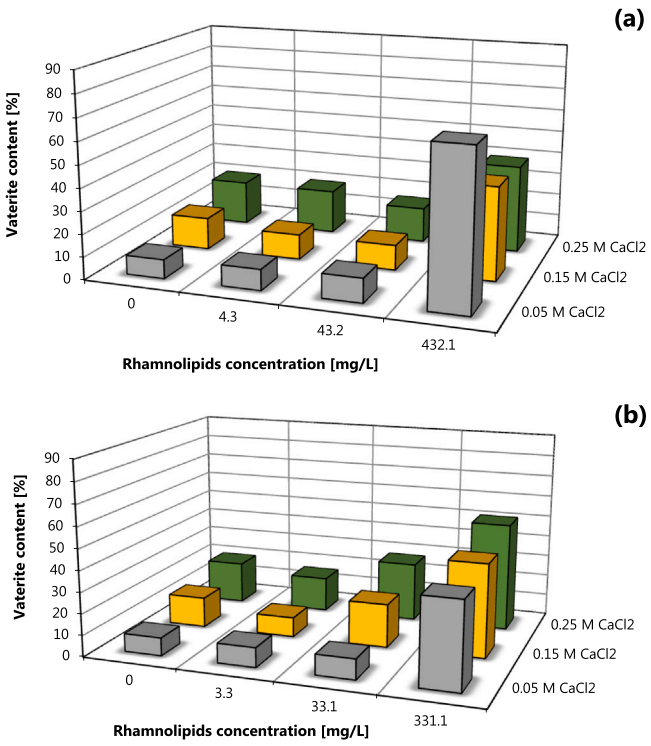

Fig. 4. Graphs showing the content of vaterite in the obtained $CaCO_3$ samples depending on the concentration of RLs and $CaCl_2$ for (a) precipitation with hydrogels containing RLs and (b) precipitation with Na_2CO_3 solution containing RLs.

plane bending oscillation of the C–O bond, and is in the range of 890–870 cm^{-1}. The last characteristic band is in the range of 1420–1450 cm^{-1} and is an asymmetric stretching band, which comes from the internal oscillation of CO_3^{2-} ions [56]. This confirms that the obtained samples consist of calcium carbonate.

Fig. S5 presents the FTIR-ATR spectra of sodium alginate and rhamnolipids. The sodium alginate spectrum shows two intense bands corresponding to symmetric and asymmetric valence vibrations of C–O in the carboxylic ion, at 1611 and 1416 cm^{-1}, respectively. In the 3000–3500 cm^{-1} range, a characteristic band is visible for the –OH group [57]. On the other hand, in the spectrum of rhamnolipids, two characteristic absorption bands can be observed, at 3269 cm^{-1} for the C-H bond, and for the –OH group at a value of 3400 cm^{-1}. The characteristic band also occurs at the value of 2925 cm^{-1} and comes from the symmetrical and asymmetrical stretching of the C-H group. The band around 1377 cm^{-1} corresponds to the asymmetric stretching of the carboxyl group. Although the band at about 1034 cm^{-1} corresponds to the vibrations of the –C–O–C– group in the cyclic structures of carbohydrates and confirmed the presence of bonds formed between the carbon atom and the hydroxyl groups in the chemical structures of the rhamnose rings [58].

Analysis of the FTIR-ATR spectra of calcium carbonate particles obtained from alginate hydrogels in the presence of rhamnolipids shows that there is a lack of characteristic bands for both alginate and rhamnolipids in the FTIR-ATR spectra of the precipitated $CaCO_3$. However, to confirm the presence of organic residues in the obtained particles, thermogravimetric analysis was performed. The TG and DTG curves of all calcium carbonate particles obtained are presented in Figs. S6 and S7 (Supplementary Materials), respectively. The DTG curves show three peaks corresponding to adsorbed water removal (small peak with a maximum around 100 °C), organic molecules removal (maximum around 240 °C) and calcium carbonate decomposition (large peak with a maximum above 700 °C). Similar courses of DTG curves were observed for calcium carbonate samples with adsorbed fatty acids [59] or

obtained in liposomes [60]. On the basis of this analysis, it is found that the content of adsorbed organic compounds in the obtained products is in the ranges of 0.53–1.47% and the largest mass of adsorbed biosurfactant molecules was for the highest rhamnolipid concentrations used, both in the solution and in the alginate hydrogel.

3.3.3. Specific surface area and pore volume

The bar graphs containing the values of the specific surface area of the precipitated $CaCO_3$ particles depending on the concentration of rhamnolipids in the hydrogel or 0.15 M Na_2CO_3 are shown in Fig. 5. In the case of control processes, that is, without the addition of rhamnolipids, an increase in the specific surface area of calcium carbonate is observed with an increase in the concentration of $CaCl_2$ in the cross-linking solution, while the difference between the specific surface area of particles obtained from cross-linked hydrogels in a solution with a concentration of 0.15 and 0.25 M is not significant. The addition of rhamnolipids to both the hydrogel and the carbonate solution in the case of using 0.05 M $CaCl_2$ increases the value of the specific surface area. The higher the RL concentration, the greater the specific surface area. However, for $CaCl_2$ concentrations of 0.15 and 0.25 M, the addition of rhamnolipids with a concentration below CMC and equal to CMC to the hydrogel reduces the value of the specific surface area of the particles compared to the control samples. The highest value was obtained for the samples obtained from the hydrogel containing rhamnolipids with a concentration above CMC and ionically cross-linked with a 0.05 M $CaCl_2$ solution. Moreover, a different relationship was observed for experiments carried out with the use of hydrogels containing biosurfactants with a concentration exceeding CMC. Contrary to the other series of experiments, in this case, a decrease in the value of the specific surface area is observed with an increase in the concentration of calcium ions. The addition of rhamnolipids to the carbonate solution does not cause such an effect.

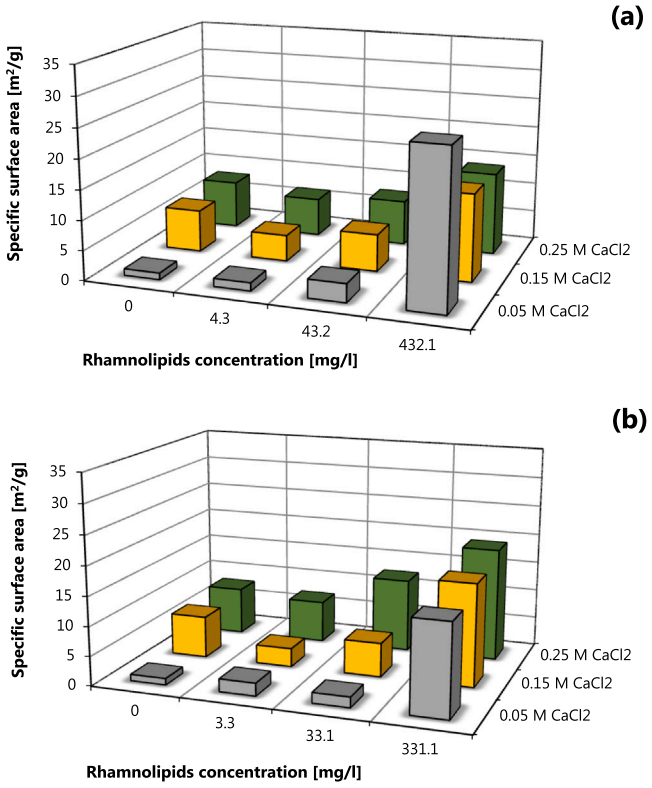

Fig. 5. Graphs showing the specific surface area of precipitated $CaCO_3$ depending on the concentration of RLs and $CaCl_2$ for (a) precipitation with hydrogels containing RLs and (b) precipitation with Na_2CO_3 solution containing RLs.

Fig. S8 shows the bar graphs containing the values of the pore volume of the rhamnolipid concentration in the hydrogel and 0.15 M Na_2CO_3. The pore volume values are correlated with the specific surface area values of the obtained particles; therefore, the same dependence of these parameters on the concentration of both rhamnolipids and calcium chloride is observed.

3.3.4. Particle size

The size distributions of calcium carbonate particles formed in the alginate hydrogel are shown in Fig. S9. During the measurements, the particles obtained in the presence of higher concentrations of rhamnolipids were hardly dispersed in water, which confirmed the adsorption of some of the biosurfactant molecules on the calcium carbonate surface. The particle size distributions are bimodal for most products. The maximum of the first peak is around 700 nm. The content of the smallest particles is less than 2% by volume. The maxima of the second peak corresponds to the main particle population. The diameters of the median distribution for all products obtained are shown in Table 1. In the control sample, performed without rhamnolipids, the size of precipitated calcium carbonate particles increased with the increasing concentration of calcium ions used for hydrogel cross-linking. When the alginate hydrogel was produced with the addition of rhamnolipids, the particle size decreased with the increasing biosurfactant concentration, and the greatest effect of rhamnolipids on particle size was seen at its highest concentration in the hydrogel. On the other hand, when rhamnolipids were added to the sodium carbonate solution, the particle size increased with increasing concentration of the biosurfactant in the solution. The size of the calcium carbonate particles in the tested system is primarily influenced by two factors: supersaturation and the presence of additives that stabilize the $CaCO_3$ crystals. Supersaturation depends on the concentration of calcium ions immobilized in the alginate hydrogel and the concentration of carbonate ions diffusing from the solution into the hydrogel. When rhamnolipids are added to the hydrogel, then the amount of Ca^{2+} ions immobilized in the resulting structure is greater. This is due to the possibility of creating additional sites for calcium ion uptake by biosurfactant molecules in the hydrogel [39]. Additionally, the amount of trapping Ca^{2+} ions also increases with increasing concentration of these ions in the solution used as an ionic cross-linking agent. The transport of carbonate ions is dependent on the cohesiveness of the hydrogel. The increase in the cohesion of the hydrogel

Table 1
The median diameter (d_{50}) of precipitated $CaCO_3$ particles and the number of Ca^{2+} moles present in the hydrogel per 1 g of alginate, depending on RLs concentration.

RLs location	RLs concentration [mg/L]	$CaCl_2$ concentration [mol/L]	Ca^{2+} present in the hydrogel [mol/g Alg]	d_{50} [nm]
Control	0	0.05	0.0017	18.6
	0	0.15	0.0036	22.9
	0	0.25	0.0040	24.4
Hydrogel	4.3	0.05	0.0019	19.2
	43.2		0.0020	17.4
	432.1		0.0022	12.9
	4.3	0.15	0.0040	21.2
	43.2		0.0044	20.7
	432.1		0.0047	18.3
	4.3	0.25	0.0053	27.8
	43.2		0.0061	26.6
	432.1		0.0071	17.7
$Na_2CO_{3(aq)}$ solution	3.3	0.05	0.0017	21.7
	33.1			18.1
	331.1			18.3
	3.3	0.15	0.0036	19.4
	33.1			22.6
	331.1			21.5
	3.3	0.25	0.0040	27.2
	33.1			27.0
	331.1			38.0

depends on both the concentration of calcium ions and the concentration of the biosurfactant. For a fixed concentration of calcium ions, the cohesiveness of the gel increased with decreasing concentration of biosurfactant. This may slow down the diffusion of calcium ions and, consequently, reduce supersaturation. In addition, a higher concentration of biosurfactant in the hydrogel may stabilize the small crystals formed; therefore, a decrease in calcium carbonate particles is observed with an increase in the concentration of the biosurfactant added to the hydrogel. This hypothesis is also confirmed by the comparison of the size of particles obtained in hydrogels that differ in the concentration of calcium ions. In this case, the cohesiveness of the gels increases with increasing Ca^{2+} concentration, which hinders the transport of carbonate ions. As a result, the obtained supersaturation is smaller and the $CaCO_3$ particles are larger. However, in the case where rhamnolipids were added to the carbonate solution, then the particle size depended primarily on the concentration of calcium ions contained in the hydrogel and increased with increasing their concentration. Furthermore, in the case of calcium ion concentrations of 0.05 and 0.15 M, the effect of rhamnolipids on particle size was small. A significant increase in the size of calcium carbonate particles was observed when precipitation was carried out in the hydrogel containing the highest concentration of calcium ions using the carbonate solution with the highest concentration of biosurfactant. In this case, the stabilizing effect of a high concentration of rhamnolipid molecules is demonstrated, which enables the formation of large particles of metastable vaterite.

3.3.5. Morphology

SEM micrographs showing $CaCO_3$ crystals precipitated using a hydrogel cross-linked with 0.05 M $CaCl_2$ depending on the concentration and location of the RLs are presented in Fig. 6. While micrographs of samples obtained in experiments with the use of 0.15 and 0.25 M $CaCl_2$ solution as a cross-linking agent are shown in the Supplementary Materials in Figs. S10 and S11, respectively. On this basis, it can be concluded that the obtained particles are a mixture of two polymorphs of calcite and vaterite. The micrographs show that vaterite occurs in the form of spherical particles with a very porous surface, whereas calcite mainly forms rhombohedral particles with a smooth surface. In addition, calcium carbonate particles formed an aggregate and often have deformed shapes.

3.4. Precipitation mechanism

The single diffusion solution phase reactant method is characterized by mild precipitation conditions, mapping the process of biomineralization in living organisms. In such a reaction system, calcium ions are released from the hydrogel, while carbonate ions are components of the aqueous solution. Calcium carbonate precipitation using Ca^{2+} loaded hydrogels depends on two equilibria, that is, the $CaCO_3$ solubility product constant and calcium alginate gelation [61]. In the precipitation process using Ca^{2+} loaded hydrogels, alginate affects the nucleation and growth of $CaCO_3$ crystals through the chemical interaction of the hydrogel with the mineral phase [62], and it is possible to precipitate various $CaCO_3$ polymorphs using an alginate template [63]. This is because alginate matrices contain charged and polar functional groups, which can interact with diffusing solutes such as Ca^{2+} and CO_3^{2-}. Consequently, this leads to a change in the concentration of the local reagents, i.e., supersaturation. In the hydrogel reaction environment, as in organic matrices in biological systems, laminar flow, Brownian motion, and convection currents are suppressed. Therefore, diffusion is the dominant mass transport mechanism [64]. Furthermore, additional substances present directly in the hydrogel or in the ambient environment also influence the characteristics of the precipitated particles. The studies of calcium carbonate precipitation in hydrogels indicate that the $CaCO_3$ polymorph formed depends on the hydrogel composition. Higher xanthan concentration in hydrogels resulted in the formation of calcium carbonate with a higher vaterite content in the mixture of calcite and vaterite polymorphs [63]. Introducing -COOH groups into the hydrogel network (copolymer of poly-acrylamide and acrylic acid) promoted nucleation and temporarily stabilized vaterite crystals [65]. However, amorphous calcium carbonate (ACC) (the least stable calcium carbonate form) was precipitated in double network hydrogel [66]. It was shown that the composition ratio of the monomers used in the production influenced the concentration of the obtained ACC [67]. In addition, the selection of the appropriate proportions of N-(phosphonomethyl) glycine (PMGly) and $MgCl_2$ added to the double network hydrogels regulated the formation of polymorphic forms of calcium carbonate. The higher concentrations of PMGly effectively inhibited the transformation of ACC into stable crystalline calcium carbonate forms [66]. Other tested substances added to the hydrogel were polyaspartic acid (PAsp) and polylysine (PLys) [68]. The presence of PLys alone into the agar hydrogel resulted in the formation of calcite particles with the morphology of star-like shaped dendrites, and a small amount of spherical vaterite. The addition of PAsp alone or a mixture of PAsp and PLys led to the crystallization of calcium carbonate in the form of spherulites with a hierarchical structure (inner core with looser outer part). The functional groups of both alginate and additives can interact directly with the crystals facets influencing the crystals nucleation and growth. Thus, the formation of crystals in hydrogels and with the addition of rhamnolipids to the reaction environment as a model biomineralization system allows us to study the mechanisms of crystal formation in bacterial biofilms [64].

The proposed mechanism of $CaCO_3$ precipitation in alginate hydrogel containing rhamnolipids is shown in Fig. 7. In the case of precipitation in the hydrogel-liquid system, crystals are formed on the surface of the hydrogel, i.e., in the place closest to the aqueous carbonate solution [64]. As a result of the gradual diffusion of CO_3^{2-} ions into the hydrogel, a reaction between carbonate and calcium ions takes place, resulting in the formation of $CaCO_3$ crystals. The consequence of this is the breakdown of the alginate hydrogel as a result of the removal of calcium ions from it and their replacement with Na^+ ions. With the course of precipitation, a kind of transition layer between the aqueous solution and the hydrogel grows (light yellow area in Fig. 7). This layer consists of the resulting $CaCO_3$ particles and sodium alginate gradually dissolving in water. This soluble process occurs very slowly, especially in a system where the solution is not mixed. The resulting layer of sodium alginate, to some extent, immobilizes the crystals formed, which may lead to their agglomeration.

The combination of the two media containing Ca^{2+} and CO_3^{2-} ions results in the formation of nuclei and then nanoparticles of the precursor phase, i.e., amorphous calcium carbonate (ACC) [69]. This phase is characterized by a high degree of hydration and is indicated as the least stable form of calcium carbonate. ACC particles formed in solution are equilibrated in a few seconds and thus converted to vaterite particles by direct solid state transformation, which is experimentally very difficult to capture [70]. It has been shown that during crystallization, vaterite can have a positive charge on the surface [69]. Negatively charged hydroxyl groups present in rhamnolipid molecules (see Fig. 8) can adsorb on the surface of the formed vaterite particles and change the surface energy. This phenomenon provides for the stabilization of this polymorphic form by protecting it from transformation to more stable forms. Furthermore, the presence of rhamnolipids in the reaction system changes the solubility of vaterite, which results in a slowdown in the transformation of this polymorph to calcite.

4. Conclusions

In this research, the single diffusion solution phase reactant method characterized by mild precipitation conditions that mapping the process of biomineralization in living organisms has been applied. It has been shown that the presence of rhamnolipids influences the consumption of calcium ions during cross-linking, effectively increasing this parameter. This effect is observed regardless of whether the biosurfactant is present

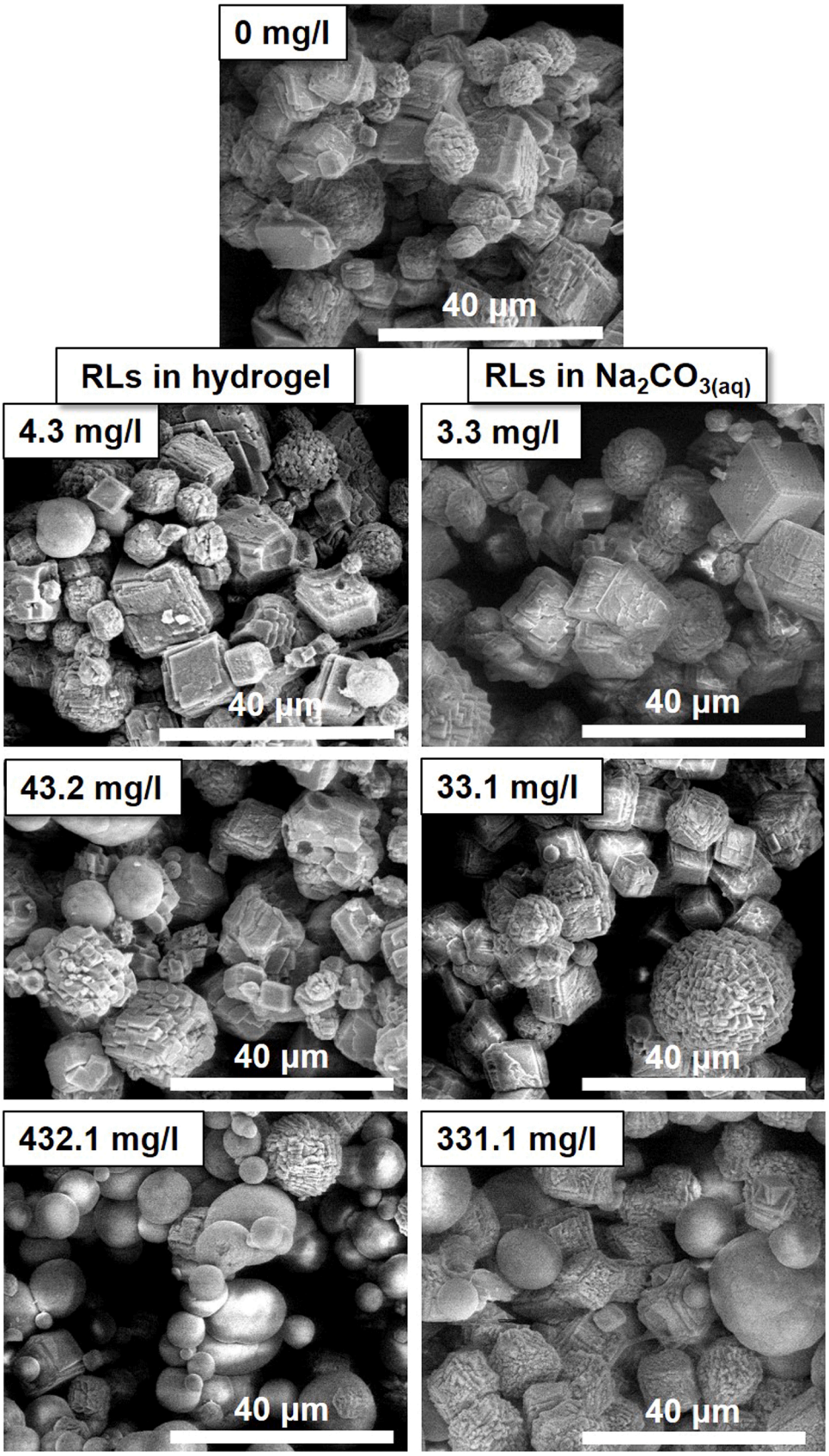

Fig. 6. SEM micrographs (2000x magnification) of $CaCO_3$ samples precipitated using hydrogel cross-linked with 0.05 M $CaCl_2$ depending on the concentration and location of RLs.

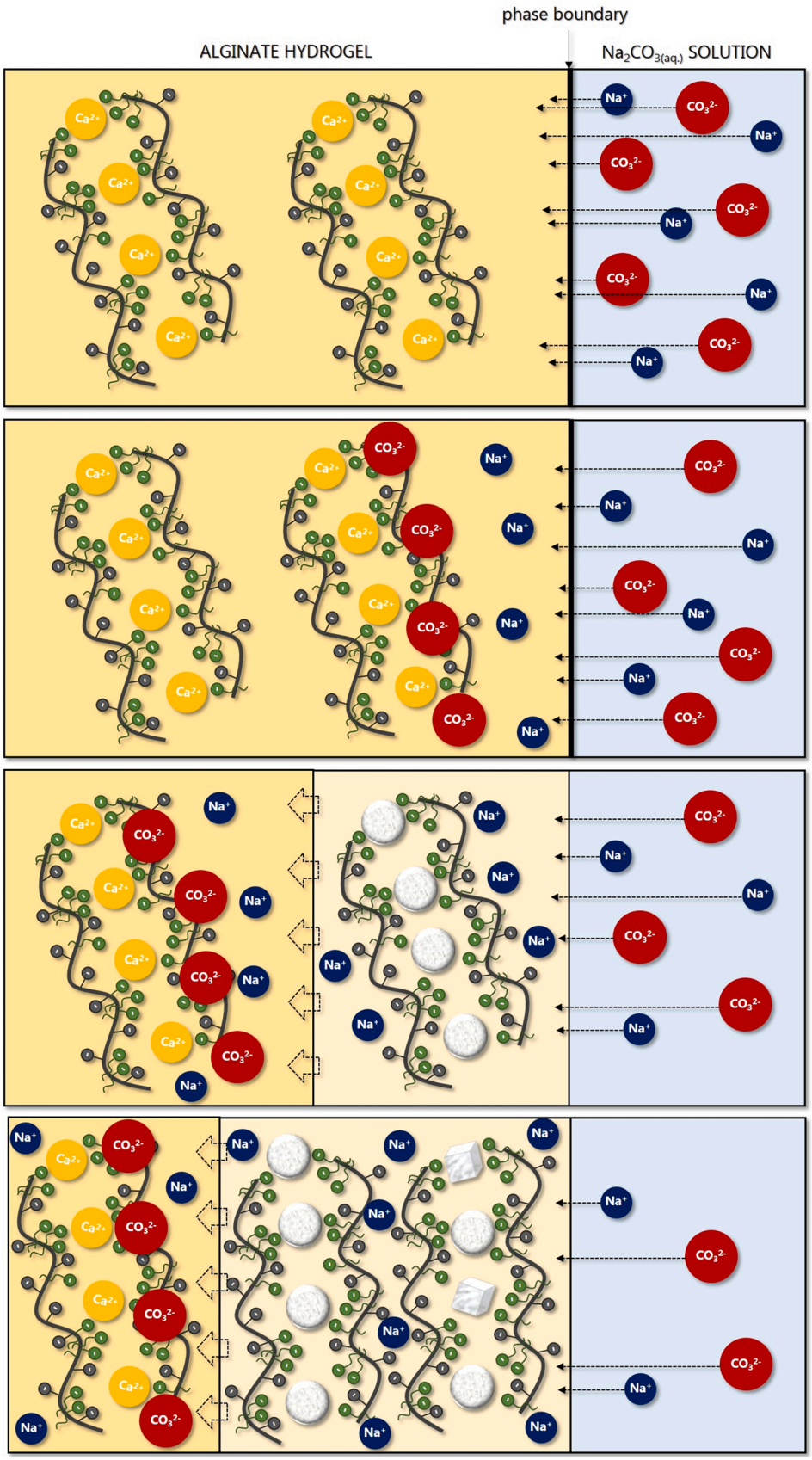

Fig. 7. Proposed mechanism of $CaCO_3$ precipitation in alginate hydrogel containing rhamnolipids (dark yellow area – alginate hydrogel, light yellow area – precipitation region, blue area – carbonate aqueous solution).

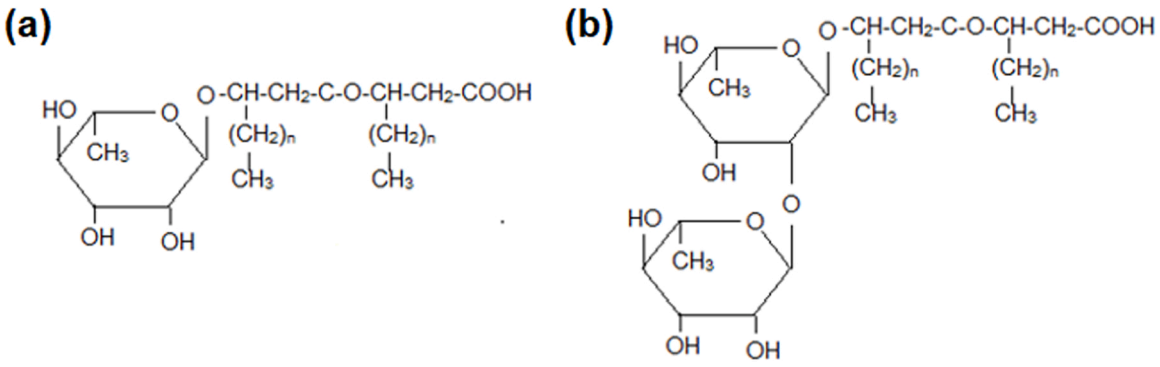

Fig. 8. Chemical structure of monorhamnolipids (a), and dirhamnolipids (b).

in the solution in free form or the form of micelles. Furthermore, the results of this research show that rhamnolipids have an effect on the characteristics of precipitated calcium carbonate in a system that simulates the biomineralization environment. Importantly, the effect of these biosurfactants depends on their concentration, as well as whether they are directly in the hydrogel matrix or the carbonate solution surrounding the hydrogel. The greatest effect compared to control samples is the presence of rhamnolipids in the form of micelles directly in the hydrogel with the $CaCl_2$ cross-linked solution at a concentration of 0.05 M, as it results in the highest increase in vaterite content, specific surface area and pore volume. The mechanism of $CaCO_3$ precipitation in alginate hydrogel containing rhamnolipids has also been proposed.

Funding

This research received no external funding.

CRediT authorship contribution statement

N.C. and D.K.-Ł.: Conceptualization. **N.C.**: Methodology. **N.C.**: Formal analysis. **N.C., A.N., A.M.-G., M.Ł. and R.B.**: Investigation. **N.C.**: Data curation. **N.C.**: Writing – original draft. **D.K.-Ł.**: Writing – review & editing. **N.C. and A.N.**: Visualization. **D.K.-Ł.**: Supervision. All authors have read and agreed to the published version of the manuscript.

Declaration of Competing Interest

The authors declare no conflict of interest.

Data availability

No data was used for the research described in the article.

Appendix A. Supporting information

Supplementary data associated with this article can be found in the online version at doi:10.1016/j.colsurfb.2022.112749.

References

[1] P. Dobryszycki, R. Hołubowicz, A. Porębska, M. Poznar, M. Różycka, Biomineralization – precision of shape, structure and properties controlled by proteins, Post. Biochem. 61 (2015) 364–380.
[2] K. Simkiss, K.M. Wilbur, Biomineralization. Cell Biology and Mineral Deposition, Elsevier, 2012.
[3] S. Mann, Biomineralization: Principles and Concepts in Bioinorganic Materials Chemistry, Oxford University Press, 2001.
[4] L.B. Gower, Biomimetic model systems for investigating the amorphous precursor pathway and its role in biomineralization, Chem. Rev. 108 (2008) 4551–4627, https://doi.org/10.1021/cr800443h.
[5] D.B. Trushina, T.V. Bukreeva, M.N. Antipina, Size-controlled synthesis of vaterite calcium carbonate by the mixing method: aiming for nanosized particles, Cryst. Growth Des. 16 (2016) 1311–1319, https://doi.org/10.1021/acs.cgd.5b01422.
[6] R. Beck, J.P. Andreassen, The onset of spherulitic growth in crystallization of calcium carbonate, J. Cryst. Growth 312 (2010) 2226–2238, https://doi.org/10.1016/j.jcrysgro.2010.04.037.
[7] J.D. Rodriguez-Blanco, S. Shaw, L.G. Benning, The kinetics and mechanisms of amorphous calcium carbonate (ACC) crystallization to calcite, via vaterite, Nanoscale 3 (2011) 265–271, https://doi.org/10.1039/c0nr00589d.
[8] J. Chen, L. Xiang, Controllable synthesis of calcium carbonate polymorphs at different temperatures ☆, Powder Technol. 189 (2010) 64–69, https://doi.org/10.1016/j.powtec.2008.06.004.
[9] F.F. Amos, D.M. Sharbaugh, D.R. Talham, L.B. Gower, M. Fricke, D. Volkmer, Formation of single-crystalline aragonite tablets/films via an amorphous precursor, Langmuir 23 (2007) 1988–1994, https://doi.org/10.1021/la061960n.
[10] S. Tugulu, M. Harms, M. Fricke, D. Volkmer, H.A. Klok, Polymer brushes as ionotropic matrices for the directed fabrication of microstructured calcite thin films, Angew. Chem. Int. Ed. 45 (2006) 7458–7461, https://doi.org/10.1002/anie.200602382.
[11] M. Castellanos, A. Torres-Pardo, R. Rodríguez-Pérez, M. Gasset, Amyloid assembly endows gad m 1 with biomineralization properties, Biomolecules 8 (2018) 13, https://doi.org/10.3390/biom8010013.
[12] A.M. Didyk, Z. Sadowski, Flotation of serpentinite and quartz using biosurfactants, Physicochem. Probl. Miner. Process 48 (2012) 607–618, https://doi.org/10.5277/ppmp120224.
[13] F. Arab, C.N. Mulligan, An eco-friendly method for heavy metal removal from mine tailings, Environ. Sci. Pollut. Res. 25 (2018) 16202–16216, https://doi.org/10.1007/s11356-018-1770-3.
[14] G. Dhanarajan, R. Sen, Amphiphilic molecules of microbial origin: classification, characteristics, genetic regulations and pathways for biosynthesis, in: C. N. Mulligan, S.K. Sharma, A. Mudhoo (Eds.), Biosurfactants Research and Trends Application, CRC Press Taylor & Francis Group, 2014, pp. 31–48.
[15] A. Bastrzyk, M. Fiedot-Toboła, I. Polowczyk, K. Legawiec, G. Płaza, Effect of a lipopeptide biosurfactant on the precipitation of calcium carbonate, Colloids Surf. B Biointerfaces 174 (2019) 145–152, https://doi.org/10.1016/j.colsurfb.2018.11.009.
[16] A. Bastrzyk, M. Fiedot-Toboła, H. Maniak, I. Polowczyk, G. Płaza, Surfactin as a green agent controlling the growth of porous calcite microstructures, Int. J. Mol. Sci. 21 (2020) 1–15, https://doi.org/10.3390/ijms21155526.
[17] M. Jahanbani Veshareh, E. Ganji Azad, T. Deihimi, A. Niazi, S. Ayatollahi, Isolation and screening of Bacillus subtilis MJ01 for MEOR application: biosurfactant characterization, production optimization and wetting effect on carbonate surfaces, J. Pet. Explor. Prod. Technol. 9 (2019) 233–245, https://doi.org/10.1007/s13202-018-0457-0.
[18] K. Gopal, Z. Lu, M.M. De Villiers, Y. Lvov, Composite phospholipid-calcium carbonate microparticles: influence of anionic phospholipids on the crystallization of calcium carbonate, J. Phys. Chem. B 110 (2006) 2471–2474, https://doi.org/10.1021/jp056865m.
[19] J. Xiao, Z. Wang, Y. Tang, S. Yang, Biomimetic mineralization of CaCO3 on a phospholipid monolayer: from an amorphous calcium carbonate precursor to calcite via vaterite, Langmuir 26 (2010) 4977–4983, https://doi.org/10.1021/la903641k.
[20] J. Kim, S.K. Bea, Y.H. Kim, D.W. Kim, K.Y. Lee, C.M. Lee, Improved suspension stability of calcium carbonate nanoparticles by surface modification with oleic acid and phospholipid, Biotechnol. Bioprocess Eng. 20 (2015) 794–799, https://doi.org/10.1007/s12257-014-0898-3.
[21] P. Pal, T. Kamilya, S. Acharya, G.B. Talapatra, Formation of calcium carbonate crystal using phospholipid monolayer template under ambient condition, J. Phys. Chem. C 114 (2010) 8348–8352, https://doi.org/10.1021/jp102696s.
[22] K. Benzerara, N. Menguy, P. López-García, T.H. Yoon, J. Kazmierczak, T. Tyliszczak, F. Guyot, G.E. Brown, Nanoscale detection of organic signatures in carbonate microbialites, Proc. Natl. Acad. Sci. USA 103 (2006) 9440–9445, https://doi.org/10.1073/pnas.0603255103.

[23] X. Li, D.L. Chopp, W.A. Russin, P.T. Brannon, M.R. Parsek, A.I. Packman, Spatial patterns of carbonate biomineralization in biofilms, Appl. Environ. Microbiol. 81 (2015) 7403–7410, https://doi.org/10.1128/AEM.01585-15.
[24] Y. Bai, X. jing Guo, Y. zhen Li, T. Huang, Experimental and visual research on the microbial induced carbonate precipitation by Pseudomonas aeruginosa, AMB Express 7 (2017) 57, https://doi.org/10.1186/s13568-017-0358-5.
[25] E.E. Mann, D.J. Wozniak, Pseudomonas biofilm matrix composition and niche biology, FEMS Microbiol. Rev. 36 (2012) 893–916, https://doi.org/10.1111/j.1574-6976.2011.00322.x.
[26] M.E. Davey, G.A. O'toole, Microbial biofilms: from ecology to molecular genetics, Microbiol. Mol. Biol. Rev. 64 (2000) 847–867, https://doi.org/10.1128/mmbr.64.4.847-867.2000.
[27] M. Espinosa-Urgel, Rhamnolipids maintain fluid channels in biofilms, J. Bacteriol. 185 (2003) 699–700, https://doi.org/10.1128/JB.185.3.699.
[28] Y. Irie, G.A. O'Toole, M.H. Yuk, Pseudomonas aeruginosa rhamnolipids disperse Bordetella bronchiseptica biofilms, FEMS Microbiol. Lett. 250 (2005) 237–243, https://doi.org/10.1016/j.femsle.2005.07.012.
[29] R. Fuchs-Godec, The adsorption, CMC determination and corrosion inhibition of some N-alkyl quaternary ammonium salts on carbon steel surface in 2 M H2SO4, Colloids Surf. A Physicochem. Eng. Asp. 280 (2006) 130–139, https://doi.org/10.1016/j.colsurfa.2006.01.046.
[30] J.M. Luna, R.D. Rufino, L.A. Sarubbo, L.R.M. Rodrigues, J.A.C. Teixeira, G.M. De Campos-Takaki, Evaluation antimicrobial and antiadhesive properties of the biosurfactant Lunasan produced by Candida sphaerica UCP 0995, Curr. Microbiol. 62 (2011) 1527–1534, https://doi.org/10.1007/s00284-011-9889-1.
[31] P. Degen, M. Paulus, E. Zwar, V. Jakobi, S. Dogan, M. Tolan, H. Rehage, Surfactant-mediated formation of alginate layers at the water-air interface, Surf. Interface Anal. 51 (2019) 1051–1058, https://doi.org/10.1002/sia.6691.
[32] J. Du, A. Zhang, X. Zhang, X. Si, J. Cao, Comparative analysis of rhamnolipid congener synthesis in neotype Pseudomonas aeruginosa ATCC 10145 and two marine isolates, Bioresour. Technol. 286 (2019), 121380, https://doi.org/10.1016/j.biortech.2019.121380.
[33] I.E. Kłosowska-Chomiczewska, K. Mędrzycka, E. Hallmann, E. Karpenko, T. Pokynbroda, A. Macierzanka, C. Jungnickel, Rhamnolipid CMC prediction, J. Colloid Interface Sci. 488 (2017) 10–19, https://doi.org/10.1016/j.jcis.2016.10.055.
[34] M.N. Radzuan, I.M. Banat, J. Winterburn, Production and characterization of rhamnolipid using palm oil agricultural refinery waste, Bioresour. Technol. 225 (2017) 99–105, https://doi.org/10.1016/j.biortech.2016.11.052.
[35] M. Sánchez, F.J. Aranda, M.J. Espuny, A. Marqués, J.A. Teruel, Á. Manresa, A. Ortiz, Aggregation behaviour of a dirhamnolipid biosurfactant secreted by Pseudomonas aeruginosa in aqueous media, J. Colloid Interface Sci. 307 (2007) 246–253, https://doi.org/10.1016/j.jcis.2006.11.041.
[36] B. İkizler, G. Arslan, E. Kipcak, C. Dirik, D. Çelenk, T. Aktuğlu, Ş. Helvacı, S. Peker, Surface adsorption and spontaneous aggregation of rhamnolipid mixtures in aqueous solutions, Colloids Surf. A Physicochem. Eng. Asp. 519 (2017) 125–136, https://doi.org/10.1016/j.colsurfa.2016.06.056.
[37] G. Özdemir, S. Peker, S.S. Helvaci, Effect of pH on the surface and interfacial behavior of rhamnolipids R1 and R2, Colloids Surf. A Physicochem. Eng. Asp. 234 (2004) 135–143, https://doi.org/10.1016/j.colsurfa.2003.10.024.
[38] H. Abbasi, K.A. Noghabi, M.M. Hamedi, H.S. Zahiri, A.A. Moosavi-Movahedi, M. Amanlou, J.A. Teruel, A. Ortiz, Physicochemical characterization of a monorhamnolipid secreted by Pseudomonas aeruginosa MA01 in aqueous media. An experimental and molecular dynamics study, Colloids Surf. B Biointerfaces 101 (2013) 256–265, https://doi.org/10.1016/j.colsurfb.2012.06.035.
[39] N. Czaplicka, S. Mania, D. Konopacka-Łyskawa, Influence of rhamnolipids and ionic cross-linking conditions on the mechanical properties of alginate hydrogels as a model bacterial biofilm, Int. J. Mol. Sci. 22 (2021) 6840, https://doi.org/10.3390/ijms22136840.
[47] H. Tong, W. Ma, L. Wang, P. Wan, J. Hu, L. Cao, Control over the crystal phase, shape, size and aggregation of calcium carbonate via a L-aspartic acid inducing process, Biomaterials 25 (2004) 3923–3929, https://doi.org/10.1016/j.biomaterials.2003.10.038.
[48] S.F. Bt Ibrahim, N.A.N. Mohd Azam, K.A.M. Amin, Sodium alginate film: the effect of crosslinker on physical and mechanical properties, IOP Conf. Ser. Mater. Sci. Eng. 509 (2019), 012063, https://doi.org/10.1088/1757-899X/509/1/012063.
[49] H. Huang, Y. Lin, P. Peng, J. Geng, K. Xu, Y. Zhang, L. Ding, H. Ren, Calcium ion- and rhamnolipid-mediated deposition of soluble matters on biocarriers, Water Res. 133 (2018) 37–46, https://doi.org/10.1016/j.watres.2018.01.010.
[50] P. March, The biosurfactant developed by Pseudomonas aeruginosa is an effective metal complexing agent such as Pb2 ad, Cd2 ad and Zn2 adjacentt (2001) 479–485.
[51] R. Liu, S. Huang, X. Zhang, Y. Song, G. He, Z. Wang, B. Lian, Bio-mineralisation, characterization, and stability of calcium carbonate containing organic matter, RSC Adv. 11 (2021) 14415–14425, https://doi.org/10.1039/d1ra00615k.
[52] C.G. Kontoyannis, N.V. Vagenas, Calcium carbonate phase analysis using XRD and FT-Raman spectroscopy, Analyst 125 (2000) 251–255, https://doi.org/10.1039/a908609i.
[53] N. Czaplicka, D. Konopacka-Łyskawa, B. Kościelska, M. Łapiński, Effect of selected ammonia escape inhibitors on carbon dioxide capture and utilization via calcium carbonate precipitation, J. CO2 Util. 42 (2020), 101298, https://doi.org/10.1016/j.jcou.2020.101298.
[54] N. Czaplicka, D. Konopacka-Łyskawa, Studies on the utilization of post-distillation liquid from Solvay process to carbon dioxide capture and storage, SN Appl. Sci. 1 (2019) 431, https://doi.org/10.1007/s42452-019-0455-y.
[55] D. Konopacka-Łyskawa, N. Czaplicka, M. Łapiński, B. Kościelska, R. Bray, Precipitation and transformation of vaterite calcium carbonate in the presence of some organic solvents, Materials 13 (2020) 1–14, https://doi.org/10.3390/ma13122742.
[56] F. Leitermann, C. Syldatk, R. Hausmann, Fast quantitative determination of microbial rhamnolipids from cultivation broths by ATR-FTIR Spectroscopy, J. Biol. Eng. 2 (2008) 1–8, https://doi.org/10.1186/1754-1611-2-13.
[57] D. Sharma, Classification and Properties of Biosurfactants (2016) 21–42. https://doi.org/10.1007/978–3-319–39415-2_2.
[58] J. Huang, Z.H. Ren, Mechanism on micellization of amino sulfonate amphoteric surfactant in aqueous solutions containing different alcohols and its interfacial adsorption, J. Mol. Liq. 316 (2020), 113793, https://doi.org/10.1016/j.molliq.2020.113793.
[59] K. Kędra-Królik, M. Wszelaka-Rylik, P. Gierycz, Thermal analysis of nanostructured calcite crystals covered with fatty acids, J. Therm. Anal. Calorim. 101 (2010) 533–540, https://doi.org/10.1007/s10973-010-0853-2.
[60] A. Szcześ, D. Sternik, Properties of calcium carbonate precipitated in the presence of DPPC liposomes modified with the phospholipase A2, J. Therm. Anal. Calorim. 123 (2016) 2357–2365, https://doi.org/10.1007/s10973-015-4958-5.
[61] B. Leng, F. Jiang, K. Lu, W. Ming, Z. Shao, Growth of calcium carbonate mediated by slowly released alginate, CrystEngComm 12 (2010) 730–736, https://doi.org/10.1039/b909413j.
[62] Y. Ma, Q. Feng, Alginate hydrogel-mediated crystallization of calcium carbonate, J. Solid State Chem. 184 (2011) 1008–1015, https://doi.org/10.1016/j.jssc.2011.03.008.
[63] C. Kosanović, S. Fermani, G. Falini, D. Kralj, Crystallization of calcium carbonate in alginate and xanthan hydrogels, Crystals 7 (2017) 355, https://doi.org/10.3390/cryst7120355.
[64] E. Asenath-Smith, H. Li, E.C. Keene, Z.W. Seh, L.A. Estroff, Crystal growth of calcium carbonate in hydrogels as a model of biomineralization, Adv. Funct. Mater. 22 (2012) 2891–2914, https://doi.org/10.1002/adfm.201200300.
[65] O. Grassmann, P. Löbmann, Biomimetic nucleation and growth of CaCO3 in hydrogels incorporating carboxylate groups, Biomaterials 25 (2004) 277–282, https://doi.org/10.1016/S0142-9612(03)00526-X.
[66] M. Milovanovic, M.T. Unruh, V. Brandt, J.C. Tiller, Forming amorphous calcium carbonate within hydrogels by enzyme-induced mineralization in the presence of N-(phosphonomethyl)glycine, J. Colloid Interface Sci. 579 (2020) 357–368, https://doi.org/10.1016/j.jcis.2020.06.047.
[67] M. Milovanovic, L. Mihailowitsch, M. Santhirasegaran, V. Brandt, J.C. Tiller, Enzyme-induced mineralization of hydrogels with amorphous calcium carbonate for fast synthesis of ultrastiff, strong and tough organic–inorganic double networks, J. Mater. Sci. 56 (2021) 15299–15312, https://doi.org/10.1007/s10853-021-06204-6.
[68] N. Wada, N. Horiuchi, M. Nakamura, K. Nozaki, A. Nagai, K. Yamashita, Controlled crystallization of calcium carbonate via cooperation of polyaspartic acid and polylysine under double-diffusion conditions in agar hydrogels, ACS Omega 3 (2018) 16681–16692, https://doi.org/10.1021/acsomega.8b02445.
[69] X. Wang, R. Kong, X. Pan, H. Xu, D. Xia, H. Shan, J.R. Lu, Role of ovalbumin in the stabilization of metastable vaterite in calcium carbonate biomineralization, J. Phys. Chem. B 113 (2009) 8975–8982, https://doi.org/10.1021/jp810281f.
[70] J.D. Rodriguez-blanco, K.K. Sand, L.G. Benning, New perspectives on mineral nucleation and growth, New Perspect. Miner. Nucleic Growth (2017), https://doi.org/10.1007/978-3-319-45669-0.